Journal of Multidisciplinary Engineering Science and Technology (JMEST)
ISSN: 3159-0040
Vol. 2 Issue 9, September - 2015

Layer Crushing In One Cone Inertial Crusher

Simeon Savov
Department of Mining Mechanisation, Faculty of Mining Electromechanics, University of Mining and Geology "St. Ivan Rilski"
Sofia, Bulgaria
e-mail: ss.ss@abv.bg

Petko Nedyalkov
Department of Machine Elements and Non-metallic Constructions, Faculty of Mechanical Engineering, Technical University
Sofia, Bulgaria
e-mail: nedpetko@tu-sofia.bg

***Abstract*—Presented work deals with physical – mechanical parameters of crushing process in one cone inertial crusher focusing at the dependency between crushing force and specific deformation in the crushing chamber. Research inside the crushing chamber processes is made through partial factorial laboratory experiment in cone inertial crusher type KID-300. New force calculation principle is subjected in the paper with schemes and few formulations, regarding the differences in force creation process in comparison to neglecting of that in the previous researches. The output particle product analysis is used to form the principle of specific deformations in the crushing chamber. Layer stiffness and layered crushing phenomena are investigated through experimental review of dependence crushing force to specific deformations occurred in crushing chamber. The essential focus of the work is subjected over the mathematical model and analysis of that dependence which form the advanced research abilities over the crushing process physical – mechanical parameters applied in inertial crushing type machines.**

Keywords—Cone Inertial Crusher; Layer Crushing; Layer Deformation – Crushing Force Dependence; Layer Stiffness; Layer Phases

I. INTRODUCTION

Despite the fact that the theory of mineral comminution and grinding is far beyond the experimental development and usage of crushing machines. Theoretical investigation of machine to technology connection and dependences is actual. Still at the production lines are used large and reliable machines there is a place for investigation of relatively small machines with not so classical principle of operation which is targeted in this publication – one cone inertial crusher type Mekhanobr KID-300 [10, 11, 13, 14]. Cone inertial crushers are dynamical crushing machines operating with two moving cones and driven by unbalanced centrifugal vibrator [10, 11, 14]. Those machines break up material toward the principles of squash, bending, grinding and partial impact according to vibrating reaction with mixed of low and high frequency coming from inner cone. Other interesting phenomenon is the layered crushing chamber [1, 5, 7, 8], as in cone crushers type "Gyradisc". This phenomena occurs when both inner and outer cones come closer and bits of material influence each to other, forming a breakage surfaces in this crushing layer, so the machine do not break just only between the surfaces of the cones. Important influence over these phenomena is the brittleness of the material and porosity of the layer [9] (nor the strength) and that is first reason these machines crush materials with high strength. Previous researchers [6] found that layered crushing comes up in three particular phases, investigated with a special press which create the diagram "strain - specific pressure" or "deformation – crushing force" in the layer.

The basic zones of the crushing chamber of one cone inertial crusher are shown on Fig. 1.

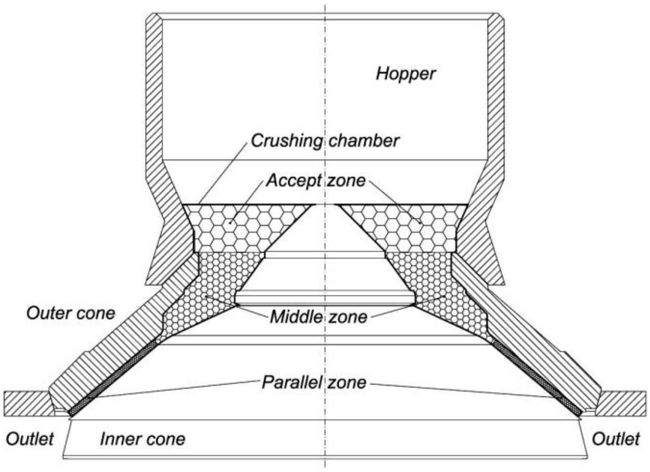

Fig. 1. *Crushing chamber of cone inertial crusher.*

II. THEORETICAL BACKGROUND

Layered crushing phases [6, 8] are describes as:

- **First phase.** The first phase reports the linear dependence between strain and specific layer pressure (or force). This is indicated with material initial compression in crushing chamber followed by crushing of particular bits of material, usually with maximal size and material reorientation in accordance to decrease material lump vacations. At the end of first phase vacancies between lumps (bits) is removed and lumps create force interaction each to other. Characterization for the end of this phase is removing of empty space (lump vacancies) and strain – specific layer pressure diagram is approximately linear.

- **Second phase.** Increasing the crushing force over that step increase the crushing process but slow down the deformation of the layer. Thus according to distribution of crushing force over more lumps (no vacancies). This create fine fractions which fill in the minimal vacations between lumps and increase layer resistance. The second phase corresponds with curvilinear strain – specific layer pressure diagram. Characteristic of this phase are volumetrically crushing of material. Sieve analysis shows clearly downsizing fractions. At the end of this phase in crushing chambers layers form zones with highly compacted fine fractions which carry the crushing force without breakage.

- **Third phase.** Far more increasing the crushing force will press the compacted zones resulting with minimal increasing of deformation and minimal crushing ratio of material. The strain – specific layer pressure diagram is approximately linear but expressively steep. Force usage and energy usage in this third phase is prior for pressing, material piece friction and fine fraction compacting, so efficiency of this phase is minimal resulting in loose of energy an mechanical overload of crusher. Therefore this phase should be minimal.

Layered crushing phases are shown on Fig. 2.

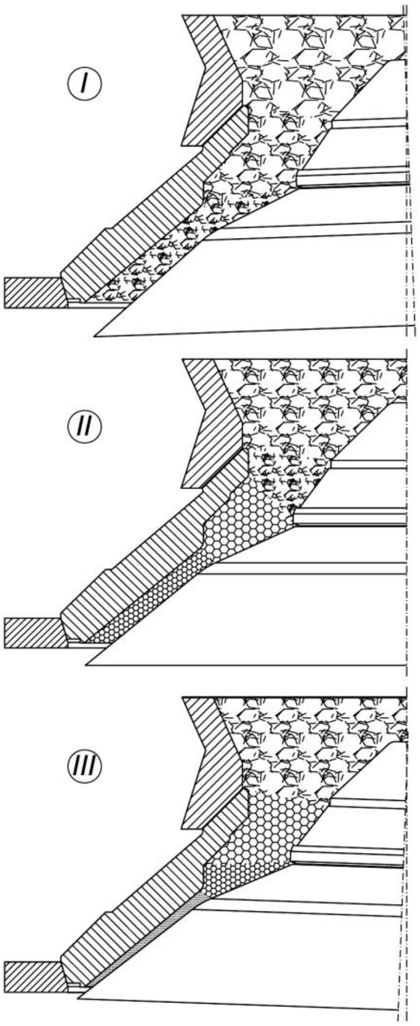

Fig. 2. *Visualization of layered crushing phases (I – the material is compression; II – the material is compacted and crushed; III – the crushed material is again compacted).*

III. Crushing Force Calculation Principle

The planar layout of forces acting over the inner cone [1, 3] is presented in Fig. 3. Calculation of crushing force F_{cr} (N), according to Fig. 3 respecting the inner cone force F_{ic} (N), force created by unbalanced centrifugal vibrator F_{ucv} (N) and geometrical parameters of crusher is:

$$F_{cr} = \frac{l_3 \cdot F_{ic} + l \cdot F_{ucv}}{l_1 \cdot \cos\gamma + l_2 \cdot \sin\gamma}, \quad N \tag{1}$$

where: l (m) – distance between spherical bearing center and rotation plane of vibrator mass center; l_1 (m) – X distance between crushing force application point and center of spherical bearing; l_2 (m) – Z distance between crushing force application point and center of spherical bearing; l_3 (m) – Z distance between inner cone force (mass center of inner cone) and center of spherical bearing; γ (deg) – cone generant (side) angle.

F_{ic} (N) – inner cone force, which is calculated by:

$$F_{ic} = \nu_{ic} \cdot m_{ic} \cdot e_1 \cdot \omega_{icp}^2, \quad N \tag{2}$$

where: ν_{ic} – coefficient rendering force loose [3, 4, 5]; m_{ic} (kg) – inner cone mass; e_1 (m) – eccentricity (distance) from precession axis of inner cone to its mass center; ω_{icp} (rad/s) – angular speed of inner cone precession.

F_{ucv} (N) – unbalance centrifugal vibrator force, which is calculated by:

$$F_{ucv} = \nu_{ucv} \cdot m_{cv} \cdot e \cdot \omega_{cv}^2, \quad N \tag{3}$$

where: ν_{ucv} – coefficient rendering force loose [3, 4, 5]; m_{cv} (kg) – centrifugal vibrator mass; e (m) – eccentricity (distance) from rotation axis of centrifugal vibrator to its mass center; ω_{cv} (rad/s) – angular speed of centrifugal vibrator.

IV. Deformation Calculation Principle

Material deformation (deformation of the layer) Δl (mm) can be calculated by:

$$\Delta l = \frac{b}{2} - h, \quad mm \tag{4}$$

where: b (mm) – static discharge opening width; h (mm) – mean value of material layer width.

Material layer stiffness is calculated by:

$$c_l = \frac{F_{cr}}{\Delta l}, \quad \frac{N}{mm}\left(\frac{kN}{m}\right) \tag{5}$$

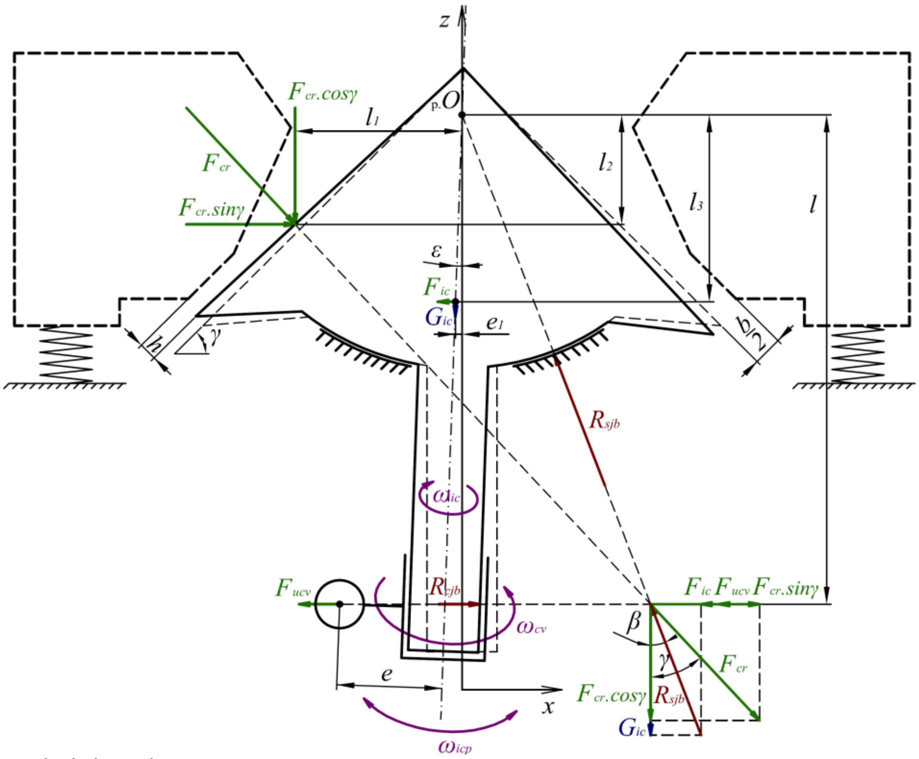

Fig. 3. *Crushing force calculation scheme.*

V. EXPERIMENTAL BACKGROUND

Research is made in laboratory of "Granulometric preparation of raw materials" in University of Mining and Geology "St. Ivan Rilski" – Sofia with cone inertial crusher type KID-300 [13, 14] using washed, sieved and dried river gravel (mix of basalt, quartz, granite and sandstone). The experiment is fractional four factor with forty test realizations using the factors as follows:

- angular speed of centrifugal vibrator – ω_{cv} (rad/s);
- mass static moment of centrifugal vibrator – S_{cv} (kg·m);
- static discharge opening width – b (mm);
- average size of input material – D_i (mm);

These factors and experimental data formulate the crushing force, material layer deformation, stiffness and etc.

Output material is sieved and analyzed [2] with respect for mean (output average diameter) value of particle diameter d_{oa} (mm) in each test realization. Analysis of the crushing process here follows particular idealization which equals the material output average diameter d_{oa} (mm) with mean value of compressed material layer width h (mm). Table 1 present result from particle analysis d_{oa} (mm), force F_{cr} (N) calculated according to (1), (2) and (3), layer deformations Δl (mm) according to (4) and layer stiffness c_l (kN/m) according to (5) for each of the test realization. Experimental and calculated values (shown in table 1) give the diagrams of (shown on Fig. 4) dependence between layer deformation and force acting on it (crushing force), which is layer stiffness graphical representation. The three distinguish lines are formed according to different static discharge opening width. Layer stiffness depends from deformations in the layer and from initial layer absolute width (b/2) which distinguish lines systematized in three groups for b=4, 6 and 8 mm.

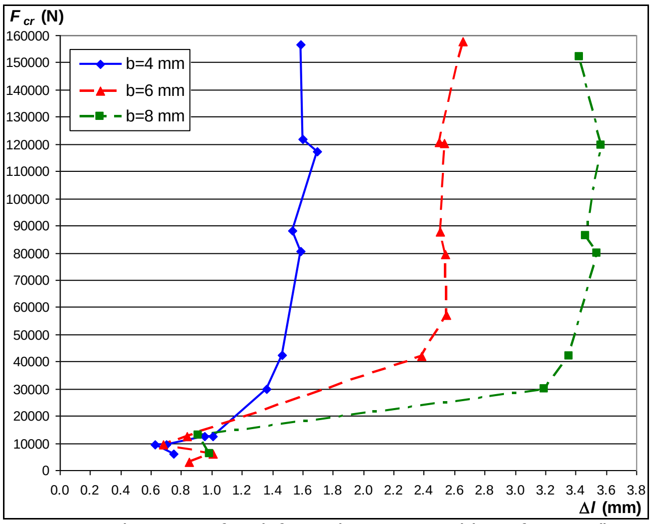

Fig. 4. *Diagram of "deformation – crushing force" (layer stiffness) for experimental work with KID-300.*

VI. RESEARCH MODELING OF LAYER STIFFNESS

Based on experimental data obtained from forty working regime test realizations with KID-300 are composed regression mathematical models to study the characteristics (theoretical and experimental) of layer stiffness. The models are made and researched with the computer program for statistical analysis STATGRAPHICS Centurion XV [15]. The best regression characteristics of layer stiffness are obtained for logarithmic function and power grade function without included constant.

According to the experimental data (table 1 and Fig. 4) the force to deformation dependence is approximated with smooth mathematical functions. Approximations are made with different functions:

- At Fig. 5 is shown approximation in absolute units (mm, N) with logarithmic function of type:

$$\Delta l = A \cdot \ln^2(F_{cr}), \quad mm \quad \Leftrightarrow \quad F_{cr} = e^{\sqrt{\frac{\Delta l}{A}}}, \quad N \qquad (6)$$

where A in this case is a coefficient depending on the value of static discharge opening width value b (mm) for logarithmic interpolation law.

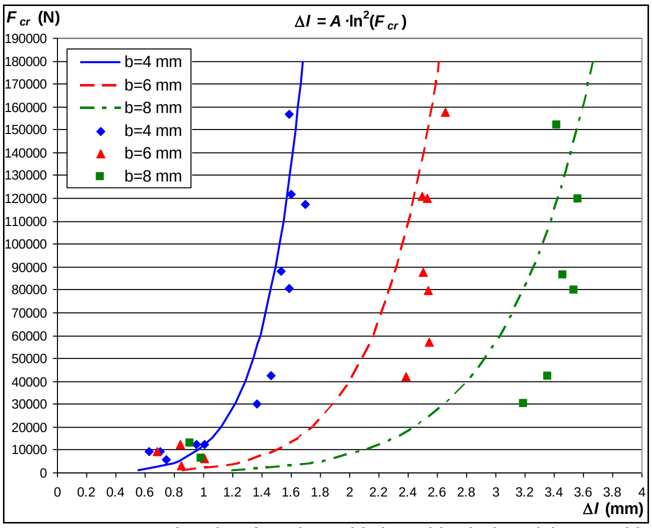

Fig. 5. *Approximation function with logarithmic law (shown with lines) – models №1, №2 and №3 (table 1) and experimental data (dots).*

- At Fig. 6 is shown approximation in absolute units (mm, N) with power grade function (biquadratic root) of type:

$$\Delta l = A \cdot \sqrt[4]{F_{cr}}, \quad mm \quad \Leftrightarrow \quad F_{cr} = \frac{1}{A^4} \cdot \Delta l^4, \quad N \qquad (7)$$

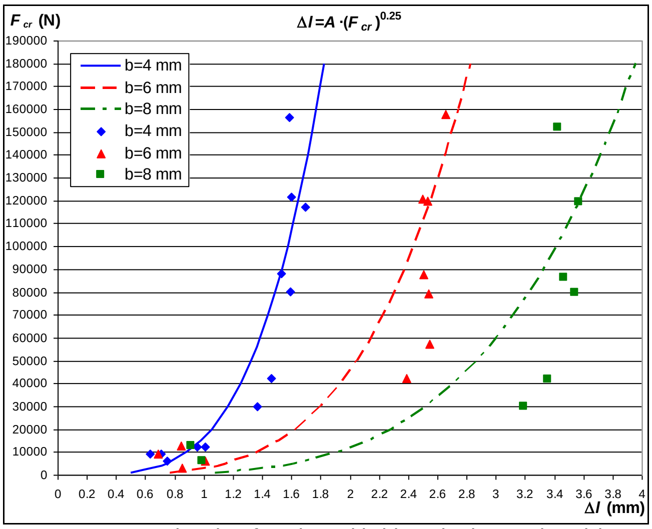

Fig. 6. *Approximation function with biquadratic root law (shown with lines) – models №4, №5 and №6 (table 1) and experimental data (dots).*

where A in this case is a coefficient depending on the value of static discharge opening width value b (mm) for biquadratic root interpolation law.

Table 2 presents statistical parameters of approximation functions noted above. A few developed variants lead to the models with improved statistical parameters – coefficient of multiple determination (R^2) over 95 %, a good values about model *F-Ratio* and model acceptance *P-Values* bellow 0.05 (5 %) – shown in following table. The table 2 also presents value comparison between logarithmic law (models №1, №2 and №3), and biquadratic root law (models №4, №5 and №6).

TABLE II. APPROXIMATION FUNCTIONS PARAMETERS

№		b	R^2 & $R^2(adj)$	F-Ratio	P-Value	A
		mm	%	-	-	-
1	logarithmic model (absolute units)	4	98.63	791.5	0.000	1.150E-02
2		6	96.10	246.5	0.000	1.787E-02
3		8	95.38	144.5	0.000	2.505E-02
4	biquadratic root law (absolute units)	4	98.94	1023.8	0.000	8.865E-02
5		6	97.19	346.5	0.000	1.371E-01
6		8	96.08	171.6	0.000	1.921E-01
7	biquadratic root law (relative units)	4	98.94	1022.4	0.000	13.968
8		6	97.20	346.7	0.000	21.610
9		8	96.08	171.5	0.000	30.268

According to Fig. 5 and Fig. 6 and table 2 can be reached the conclusion that good approximations with logarithmic and power models without initial constants in the model can be used in mathematical explanation of the layer stiffness. The coefficients of multiple determination are over 95 % which is a very good criteria for complicated engineering systems. *P-Values* of the models are below 0.05 and *F-Ratios* for all models are over hundred or few hundreds. All this statistical values lead, that such kinds of approximations are good for practical usage and experimental validation. Regression models with biquadratic root law have better parameters compared with logarithmic models (table 2) and type of the equation (7) is more convenient for practical use.

VII. LAYERING CRUSHING PHASES AND LIMITATIONS

Mathematical functions are easily researched in relatively units described bellow:

- Relatively crushing force:

Relative crushing force $F_{cr(\%)}$ (%) is calculated like a ratio between crushing force (determined by (1)) of current test realization and maximal crushing force for all test realization of the experiment:

$$F_{cr(\%)} = \frac{F_{cr(N)}}{F^{\max}_{cr(N)}} \cdot 100, \quad \% \qquad (8)$$

The values from this calculation are represented in table 1.

- Relatively crushing force:

Relative layer deformation is described like a ratio between layer deformation (determined by (4)) of current test realization and maximal theoretical layer deformation for all test realization of the experiment:

$$\Delta l_{(\%)} = \frac{\Delta l_{(mm)}}{\Delta l^{max}_{(mm)}} \cdot 100, \quad \% \tag{9}$$

Maximal theoretical layer deformation according (4) is equal to the half of the maximum static discharge opening width (b=8 mm; h=0 mm; Δl^{max}=4 mm). The values from this calculation are represented in table 1.

Graphical representations of the models in relative units (№7, №8 and №9) at b=4, 6 and 8 mm are shown on Fig. 7. These models have the same mathematical functions as models №4, №5 and №6 and their parameters are presented in table 2.

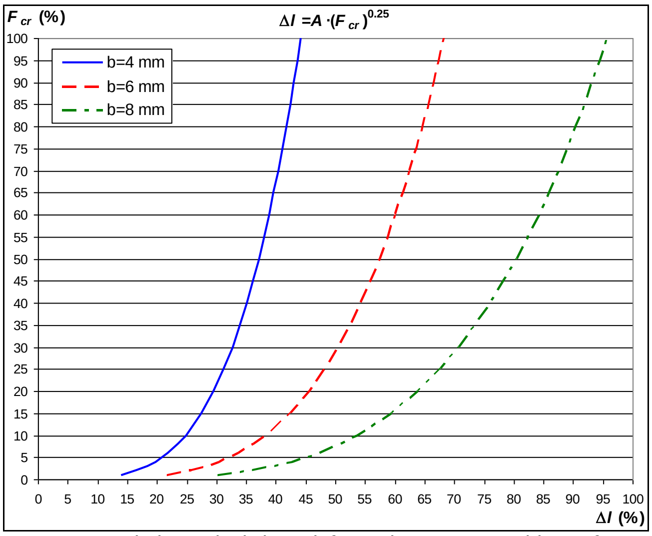

Fig. 7. *Relative (units) "deformation – crushing force" dependences for biquadratic law approximation.*

The linear or near linear parts in deformation – crushing force dependence are calculated as function derivative. It is investigated the value of tangent angle α (deg) to the abscissa coordinate (the first derivative of main function $F_{cr}=f(\Delta l)$. The equation of the researched function is:

$$F_{cr(\%)i}\left(\Delta l_{(\%)i}\right) = \frac{1}{A^4} \cdot \Delta l^4_{(\%)i}, \quad \% \tag{10}$$

And as it is described the first derivative is:

$$F'_{cr(\%)i}\left(\Delta l_{(\%)i}\right) = \frac{4}{A^4} \cdot \Delta l^3_{(\%)i} = tg\alpha_i \tag{11}$$

Relative approximation curves are researched in one hundred points (from 1 to 100 %) in which points are calculated tangent angle α (deg). The table 3 represents results with step 5 %.

So the crushing process is a physical process in functional view it is very good to find a smooth and continuous mathematical function to represent the approximation of the process. The problem came with a phase limitation borders and their determination. That is done in two ways:

A. *Subjective Linearity Acceptance*

Phase's limits acceptance are made through a hypothesis of phase (stage) linearity. Starting from first point and going further it is calculated the linearity approximation between points forming law dependence (deformation – crushing force) and linear approximation with level of subjective acceptance here R^2>99 %. For first layer crushing phase it is started from first point of the curve and for the third layer crushing phase it is started from last point of the curve and going backwards. Research from these representation shows that limits between crushing phases can be described as:

- Limit between first and second phase respectively $F_{cr(\%)}$=2.64 % *or* $F_{cr(N)}$=4168.2 N.

- Limit between second and third phase respectively $F_{cr(\%)}$=35.52 % *or* $F_{cr(N)}$=56081.2 N.

Results (in absolute units) are shown in Fig. 8 with phase limitation borders.

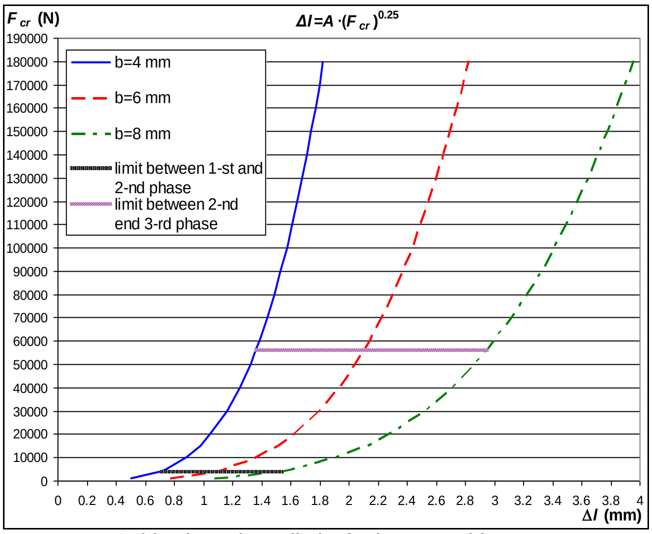

Fig. 8. *"Subjective" phase limits for layer crushing.*

In table 4 are presented the values for deformation of the layer respectively to the limits of crushing force and average angle α_{av} in linear areas (the first and third phase).

TABLE IV. Phase limits values

F_{cr} (N)	Δl (mm)			α_{av} (deg)		
	b=4 mm	*b*=6 mm	*b*=8 mm	*b*=4 mm	*b*=6 mm	*b*=8 mm
4168.2	0.712	1.102	1.543	24.36	16.38	11.88
56081.2	1.364	2.110	2.956	81.08	76.38	71.30

B. *Functional Linearity Description*

As far as it is found the mathematical representation with good statistical acceptance parameters (Fig. 6 and table 2) it can be described curvature functional representation for chosen mathematical law [12, 16]. The signed radius of curvature can be calculated with well known mathematical expression:

$$\rho_i = \frac{\sqrt{\left(1+\left(f'(\Delta l)\right)^2\right)^3}}{f''(\Delta l)}, \quad m \tag{12}$$

Which resulting in a function of following type:

$$\rho_i = \frac{B_{i1} \cdot \sqrt{\left(1+B_{i2} \cdot \Delta l^6\right)^3}}{\Delta l^2}, \quad m \tag{13}$$

Journal of Multidisciplinary Engineering Science and Technology (JMEST)
ISSN: 3159-0040
Vol. 2 Issue 9, September - 2015

where i=1, 2 and 3 are indexes depending on the value of static discharge opening width value b (mm); B_{ik} are coefficients of used approximation function.

Those curvature radiuses is represented on Fig. 9 with central line which represents the horizontal coordinate of the minimal radius value shown in same color as main diagram of curvature radius. Connection of minimal values is shown with dashed magenta line.

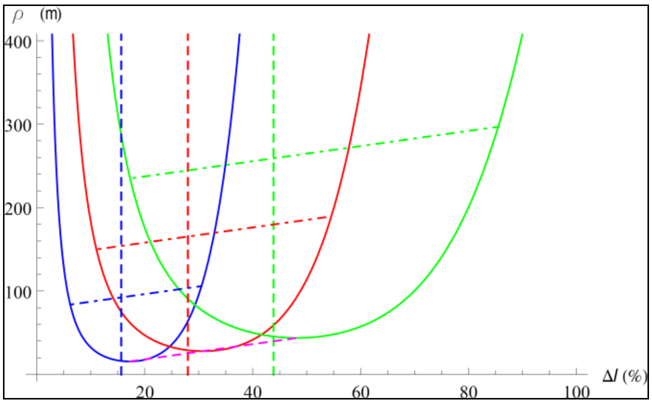

Fig. 9. *Curvature radius of main curve "deformation – crushing force" dependence radius of curvature for: b=4 mm (blue); b=6 mm (red); b=8 mm (green).*

Coordinates and parameters of those minimal values are shown in table 5.

TABLE V. CURVATURE RADIUS – COORDINATES OF MINIMAL VALUES, LEFT AND RIGHT LIMITS FOR CURVATURE

b	x_{min}	y_{min}	y/x	atan(y/x)	x_{le}	y_{le}	x_{ri}	y_{ri}
mm	%	m		deg	%	m	%	m
4	17.198	15.636	0.909	42.275	6.374	78.178	30.494	105.901
6	30.774	27.977	0.909	42.275	11.405	139.887	54.563	189.493
8	48.226	43.844	0.909	42.275	17.872	219.221	85.508	296.959

It is clearly seen on the Fig. 9 that the minimal value does not divide the curvature diagram in symmetrical sections which means that the radius of curvature is not symmetrical around its minimum value. It is calculated that angular sectors between the minimal radius values and coordinate zero is one and the same for all curves respecting of static discharge opening width and that is used to incline the left and right limit of radius growth as it is shown on Fig. 9 and table 5.

Curvature radius could be used for linearity measurement if it is described the curvature radius value over which the dependence "deformation – crushing force" can be accepted as linear. Here in this calculation (table 5) it is used a value that is five times over the minimal value. If it accepted assumption the values below the left limit and over the right limit will have a curvature radius that the determine nearly linear section, so the acceptance of linearity will be easier.

Resulting diagram for "deformation – crushing force" with phase limitations in relative units (% – %) are shown in Fig. 10. On Fig. 11 is shown the recalculated diagram "deformation – crushing force" in absolute units (N – mm).

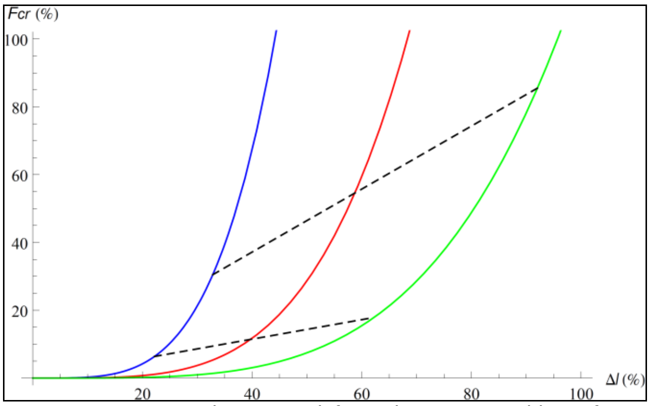

Fig. 10. *Diagram "deformation – crushing force" dependence in relative units (% – %) with phase limits for: b=4 mm (blue); b=6 mm (red); b=8 mm (green).*

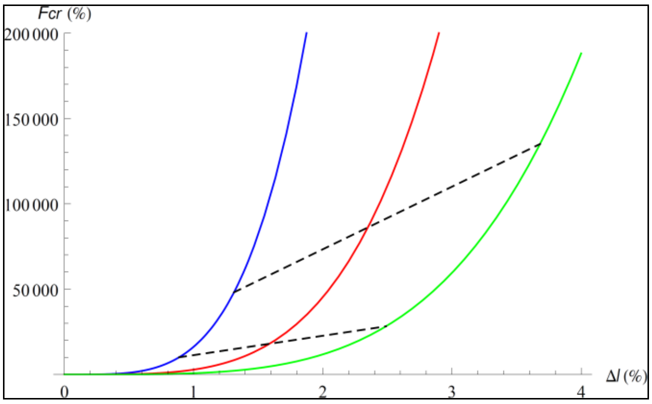

Fig. 11. *Diagram "deformation – crushing force" dependence in absolute units (N – mm) with phase limits for: b=4 mm (blue); b=6 mm (red); b=8 mm (green).*

According to this calculation way it is tried to analyze the exponential “deformation – crushing force” approximation dependence but unfortunately it is realized that this type of function is without a left asymptote and the left curvature radius is limed to some value, so the acceptance of stage linearity is contingent and not well determined.

VIII. CONCLUSIONS

There is described the methodic of calculation and investigation of crushing force to layer deformation dependence for a physical crushing machine – one cone inertial crusher. The experimental data is used for mathematical approximation of this dependence.

Mathematical interpolation functions are developed and used for analysis of layer deformation to crushing force dependences and phase separation. The authors’ opinion about preference of mathematical interpolation with polynomial function is acquittal through a curvature radius study.

A phase limitations in layer crushing dependence could be investigated and researched with methods described upwards. The functions choice for interpolation is an object of discussion realizing there is a step forward to accept or reject some of functions type.

IX. FUTURE WORK

Authors work in methods of precise experimental detection for crushing force and relative movement between the crushing cones. Changing of design plan and experimental setting will close up the experimental points and improve the interpolation and approximation, which will help in layer phases investigation.

REFERENCES

Related Work

[1] S. Savov, "Constructive-mechanical review of conical inertial crushers (KID)", Bulgarian Journal for Engineering Design, September 2012, No. 15, pp. 23-28, ISSN 1313-7530 (Text in Bulgarian)

[2] S. Savov, P. Nedyalkov and D. Mochev, "Particle size distributions of one cone inertial crusher (KID-300) products", Proceeding of XV Balkan Mineral Processing Congress, June 2013, Sozopol, Bulgaria, Vol. I, pp. 150-153, ISBN 978-954-353-218-6

[3] S. Savov, P. Nedyalkov and I. Minin, "Crushing force theoretical examination in one cone inertial crusher", Journal of Multidisciplinary Engineering Science and Technology, March 2015, Vol. 2, Issue 3, pp. 430-437, ISSN 3159-0040

Bibliography

[4] V. Arsentiev, L. Vaisberg, L. Zarogatsky and A. Shuloyakov, Production of Cubiform Crushed Stone and Road Construction Sand through the Use of Vibratory Crushers, VSEGEI, Saint-Peterburg, 2004, ISBN 93761-061-X (Text in Russian)

[5] L. Vaisberg, L. Zarogatsky and V. Turkin, Vibratory Crushers. Fundamentals of Calculation, Design and Technological Application, VSEGEI, Saint-Peterburg, 2004, ISBN 93761-061-X (Text in Russian)

[6] V. Revnivtsev, O. Barzukov, N. Ivanov, V. Laubgan, Ya. Katzman and L. Yakhkind, "Basic laws at changes of the condition of the layer of bulk material under pressure", Obogashchenie Rud, 1984, No. 4, pp. 3-6, ISSN 0202-3776 (Text in Russian)

[7] L. Bilenko, L. Blekhman, N. Rzhankova, A. Feoktistov, Ya. Shklyarskii, E. Zagrivnyi, I. Beloglazov, "Optimum parameters and methods of processing hard-alloywastes", Metallurgist, November 2008, Vol. 52, Issue 11-12, pp. 719-724, ISSN 1573-8892 [Metallurg, December 2008, No. 12, pp. 61-64, ISSN 0026-0827]

[8] A. Fedotov, G. Denisov, "Vibration Technique for Recovery of Non-Ferrous, Rare and Noble Metals from Secondary Raw Materials", EMC '91:, Non-Ferrous Metallurgy - Present and Future, September 1991, Belgium, pp. 257-263, ISBN 978-94-011-3684-6

[9] M. Zlatev, Beitrag zur quantitativen Kornformcharakterisierung unter besonderer Berücksichtigung der digitalen Bildaufnahmetechnik, Dissertation, TU Bergakademie Freiberg, 2009

[10] Russian patent: RU 2476269; SU632388 (A1)

[11] US patent: US 4655405 A; US4073446 (A)

[12] http://www.mathworld.wolfram.com

[13] http://www. mtspb.all.biz

[14] http://www.mekhanobr.spb.ru

[15] http://statgraphics.com

[16] http://www.wolfram.com

APPENDIX

TABLE I. THEORETICAL RESULTS AND EXPERIMENTAL DATA

ex.	b	d_{oa}	F_{cr}	Δl	c_l	F_{cr}	Δl	ex.	b	d_{oa}	F_{cr}	Δl	c_l	F_{cr}	Δl
№	mm	mm	N	mm	kN/m	%	%	№	mm	mm	N	mm	kN/m	%	%
16	4	1.254	5972	0.746	8005	3.78	18.65	2	6	0.614	42142	2.386	17661	26.69	59.65
22	4	1.371	9284	0.629	14771	5.88	15.71	9-15	6	0.454	57248	2.546	22485	36.26	63.65
23	4	1.295	9284	0.705	13173	5.88	17.62	19	6	0.460	79524	2.540	31308	50.37	63.50
34	4	1.047	12508	0.953	13122	7.92	23.83	27	6	0.494	87777	2.506	35029	55.59	62.65
33	4	0.992	12543	1.008	12449	7.94	25.19	31	6	0.469	120113	2.531	47466	76.08	63.26
4	4	0.635	30047	1.365	22012	19.03	34.13	30	6	0.500	120782	2.500	48322	76.50	62.49
1	4	0.538	42301	1.462	28937	26.79	36.55	38	6	0.344	157886	2.656	59441	100.00	66.40
21	4	0.410	80425	1.590	50596	50.94	39.74	18	8	3.013	6021	0.987	6102	3.81	24.67
26	4	0.470	88123	1.530	57601	55.81	38.25	36	8	3.086	12692	0.914	13892	8.04	22.84
37	4	0.306	117281	1.694	69247	74.28	42.34	5	8	0.808	30043	3.192	9411	19.03	79.81
29	4	0.403	121673	1.597	76186	77.06	39.93	3	8	0.644	42063	3.356	12535	26.64	83.89
40	4	0.414	156691	1.586	98816	99.24	39.64	20	8	0.460	79935	3.540	22583	50.63	88.49
6	6	2.150	3105	0.850	3653	1.97	21.25	28	8	0.537	86186	3.463	24884	54.59	86.59
17	6	1.992	5996	1.008	5949	3.80	25.20	32	8	0.434	119631	3.566	33549	75.77	89.15
24	6	2.317	9341	0.683	13672	5.92	17.08	39	8	0.577	152103	3.423	44431	96.34	85.58
35	6	2.160	12617	0.840	15011	7.99	21.01								

TABLE III. CALCULATION DISCRETE POINTS FOR BIQUADRATIC LAW AND IT'S TANGENT ANGLE VALUES

F_{cr} (%)	Δl (%)			$tg\alpha$			α (deg)		
	b=4 mm	*b*=6 mm	*b*=8 mm	*b*=4 mm	*b*=6 mm	*b*=8 mm	*b*=4 mm	*b*=6 mm	*b*=8 mm
1	13.97	21.61	30.27	0.286	0.185	0.132	15.98	10.49	7.53
5	20.89	32.31	45.26	0.958	0.619	0.442	43.76	31.75	23.84
10	24.84	38.43	53.83	1.610	1.041	0.743	58.16	46.15	36.62
15	27.49	42.53	59.57	2.183	1.411	1.007	65.39	54.67	45.21
20	29.54	45.70	64.01	2.708	1.751	1.250	69.73	60.26	51.34
25	31.23	48.32	67.68	3.202	2.069	1.478	72.65	64.21	55.91
30	32.69	50.58	70.84	3.671	2.373	1.694	74.76	67.15	59.45
35	33.97	52.56	73.62	4.121	2.664	1.902	76.36	69.42	62.26
40	35.13	54.35	76.12	4.555	2.944	2.102	77.62	71.24	64.56
45	36.18	55.97	78.39	4.975	3.216	2.296	78.64	72.73	66.47
50	37.14	57.46	80.49	5.385	3.480	2.485	79.48	73.97	68.08
55	38.04	58.85	82.43	5.784	3.738	2.669	80.19	75.02	69.46
60	38.88	60.14	84.24	6.174	3.990	2.849	80.80	75.93	70.66
65	39.66	61.36	85.94	6.556	4.237	3.025	81.33	76.72	71.71
70	40.40	62.51	87.55	6.930	4.479	3.198	81.79	77.42	72.64
75	41.11	63.59	89.07	7.298	4.717	3.368	82.20	78.03	73.46
80	41.77	64.63	90.52	7.660	4.951	3.535	82.56	78.58	74.20
85	42.41	65.62	91.91	8.017	5.182	3.699	82.89	79.08	74.87
90	43.02	66.56	93.23	8.368	5.409	3.862	83.19	79.52	75.48
95	43.61	67.47	94.50	8.714	5.632	4.021	83.45	79.93	76.04
100	44.17	68.34	95.72	9.056	5.853	4.179	83.70	80.31	76.54